Letter

Circumventing Scaling Relations in Oxygen Electrochemistry Using Metal−Organic Frameworks

Tyler Sours,[#] Anjli Patel,[#] Jens Nørskov, Samira Siahrostami,* and Ambarish Kulkarni*

Read Online

ACCESS | 📊 Metrics & More | 📰 Article Recommendations | 🆔 Supporting Information

ABSTRACT: It has been well-established that unfavorable scaling relationships between *OOH, *OH, and *O are responsible for the high overpotentials associated with oxygen electrochemistry. A number of strategies have been proposed for breaking these linear constraints for traditional electrocatalysts (e.g., metals, alloys, metal-doped carbons); such approaches have not yet been validated experimentally for heterogeneous catalysts. Development of a new class of catalysts capable of circumventing such scaling relations remains an ongoing challenge in the field. In this work, we use density functional theory (DFT) calculations to demonstrate that bimetallic porphyrin-based MOFs (PMOFs) are an ideal materials platform for rationally designing the 3-D active site environments for oxygen reduction reaction (ORR). Specifically, we show that the *OOH binding energy and the theoretical limiting potential can be optimized by appropriately tuning the transition metal active site, the oxophilic spectator, and the MOF topology. Our calculations predict theoretical limiting potentials as high as 1.07 V for Fe/Cr-PMOF-Al, which exceeds the Pt/C benchmark for 4e ORR. More broadly, by highlighting their unique characteristics, this work aims to establish bimetallic porphyrin-based MOFs as a viable materials platform for future experimental and theoretical ORR studies.
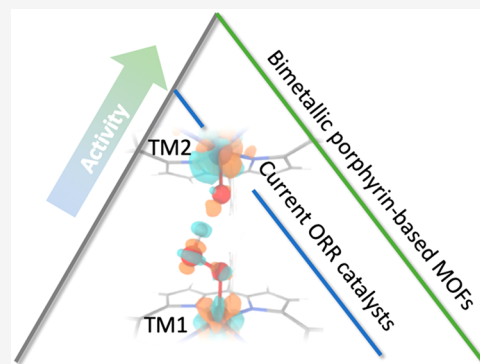
Oxygen electrochemistry in the form of oxygen reduction reaction (ORR, for fuel cells) and oxygen evolution reaction (OER, for water electrolyzers) lies at the heart of an environmentally sustainable hydrogen-based economy.[1] However, widespread adoption of these technologies has been limited due to the high cost and thermodynamic losses associated with ORR and OER electrocatalysts (referred together as OXR). Despite large research investments, only modest improvements have been achieved in catalyst performance over the past decade; the best catalysts show onset potentials that deviate ∼0.3−0.4 V away from the ideal value (i.e., 1.23 V_{RHE}).[2−4] These losses have been attributed to the unfavorable scaling between the binding energies of OXR intermediates, in particular *OOH vs *OH.[2,5,6] Although recent discoveries of low-cost alternatives are encouraging,[7,8] it is likely that their performance is also constrained by similar intrinsic limitations.

Despite slight material-specific variations, the robustness of the *OOH vs *OH linear correlation across different materials and computational methods is well-established.[9,10] Specifically, a slope of 0.9−1.0 is observed (due to the single bond with the surface) with an intercept of 2.8−3.2 eV (due to the peroxyl bond in *OOH).[5,11−14] Designing materials that circumvent this linear scaling relationship is crucial for the development of the next generation of OXR electrocatalysts.[11,15]

A promising strategy toward this goal is the confinement of *OOH within a 3-D active site environment, which has been

demonstrated for a few model systems and homogeneous molecular catalysts. For instance, Rossmeisl et al.[16,17] have shown that diporphyrin motifs are capable of facilitating *OOH dissociation via two closely spaced binding sites. This approach bypasses the limitations imposed by *OOH scaling in favor of the less restrictive dissociated *O + *OH pathway. Following some of the thermodynamic optimization guidelines discussed by Calle-Vallejo and colleagues,[18] we aim to preferentially stabilize *OOH (relative to *OH) by tuning the surrounding active site environment.

Similar to the cofacial Pacman molecules,[19−21] Figure 1 shows a related model system consisting of two transition metals (TMs). Specifically, a Fe/N_4-doped (TM_2 = Fe) graphene sheet is placed in close proximity with a TM porphyrin molecule (TM_1 = Fe, Co, and Ni). The Fe−OH center embedded in the graphene acts as an inactive spectating species that preferentially stabilizes TM_1−*OOH via hydrogen bonding interactions. An additional stabilization of 0.2−0.35 eV is observed for *OOH at distances of ∼7.0 Å (using the
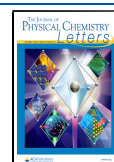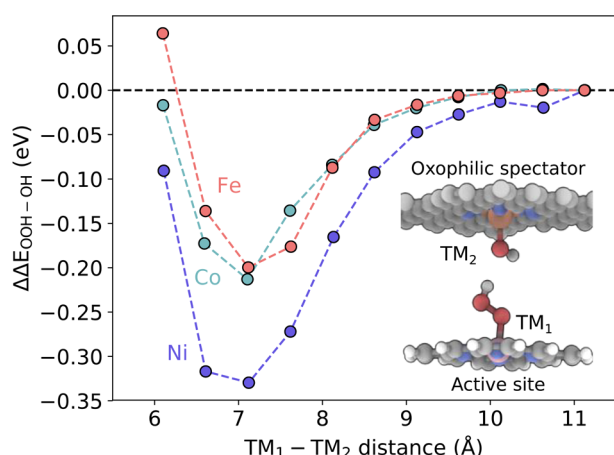
Figure 1. Preferential stabilization of *OOH relative to *OH at different distances compared to the noninteracting system for various active sites (TM_1 = Fe, red; Co, light blue; Ni, dark blue) with an oxophilic Fe−OH spectator (TM_2). $\Delta\Delta E_{OOH-OH} = \Delta E_{OOH-OH} - \Delta E^{\infty}_{OOH-OH}$, where ΔE_{OOH-OH} represents the difference between the *OOH and *OH binding energies at various TM_1-TM_2 distances and $\Delta E^{\infty}_{OOH-OH}$ represents the difference between the *OOH and *OH binding energies for the noninteracting systems (i.e., at large TM_1−TM_2 distances). The inset shows active TM_1−OOH stabilized by hydrogen-bonding interactions with TM_2−OH spectator embedded in graphene.

BEEF-vdW[22] functional) compared to the noninteracting system (i.e., at large separations). Validation with other functionals (e.g., RPBE,[23] BLYP,[24,25] B3LYP,[26] and HSE06,[27,28] with Grimme's D3BJ[29−31] dispersion correction) show that the stabilization (1) is not an artifact of using a specific functional, (2) is not dominated by van der Waals interactions (Figure S1), and (3) changes the TM_1−O bond order affecting both the slope and the intercept of the scaling lines (see Figure S2). The preferential stabilization of *OOH relative to *OH arises due to the favorable confined geometry, which provides a design principle to guide the development of active OXR catalysts.

This finding leads to an intriguing question: *can we design other materials that leverage favorable spatial orientations of binding sites to circumvent OXR scaling relations?* Although related concepts have been proposed,[32,33] to the best of our knowledge, no heterogeneous catalysts have been experimentally proven to take advantage of these effects for ORR. Within the field of electrochemistry, it is critical to translate these strategies to an experimentally synthesizable and industrially scalable class of materials.[12]

Metal−organic frameworks (MOFs), a class of nanoporous materials consisting of metal nodes interconnected by organic linkers, are uniquely attractive due to their experimentally realizable diversity of active sites, 3-D porous chemical environments, and topologies.[34−36] Although MOF electrochemistry is a relatively nascent direction, a variety of common MOFs, such as Co-PMOF-Al,[37] PCN-223(Fe),[38] PCN-226-(Co),[39] and Ni-HAB[40] show intrinsic ORR activity. The experimental onset potentials reported for these MOF systems range from 0.7−0.83 V, which is comparable with other promising catalysts. Progress in MOF electrocatalysis, including possible challenges associated with MOF stability and charge transfer, has been summarized in a number of recent reviews.[41−45]

In the remainder of this work, we use periodic density functional theory (DFT) calculations to show that bimetallic porphyrin-based, mixed-linker MOFs can be designed to preferentially stabilize *OOH. Specifically, by using a combination of active and oxophilic transition metal cations, we leverage the 3-D pore structure of MOFs to spatially orient the porphyrin binding sites and circumvent the scaling relations. We consider the full four-electron (4e) associative reduction pathway to water and the partial two-electron (2e) pathway to hydrogen peroxide (further details are presented in the Supporting Information). It should be noted that alternative mechanisms have been reported for some M−N₄ catalysts under certain conditions.[46−50] However, an exhaustive investigation into all possible mechanistic pathways is beyond the scope of this work. The theoretical limiting potential (U_L), defined as the highest potential at which all reaction steps remain thermodynamically downhill, is used to evaluate electrocatalytic performance. Although U_L is determined entirely from thermodynamics, it has been shown to correlate with ORR activity.[6]

Figure 2a shows the structure of PMOF-Al,[37,51] which consists of TCPP ligands (TCPP = tetrakis(4-carboxyphenyl)-
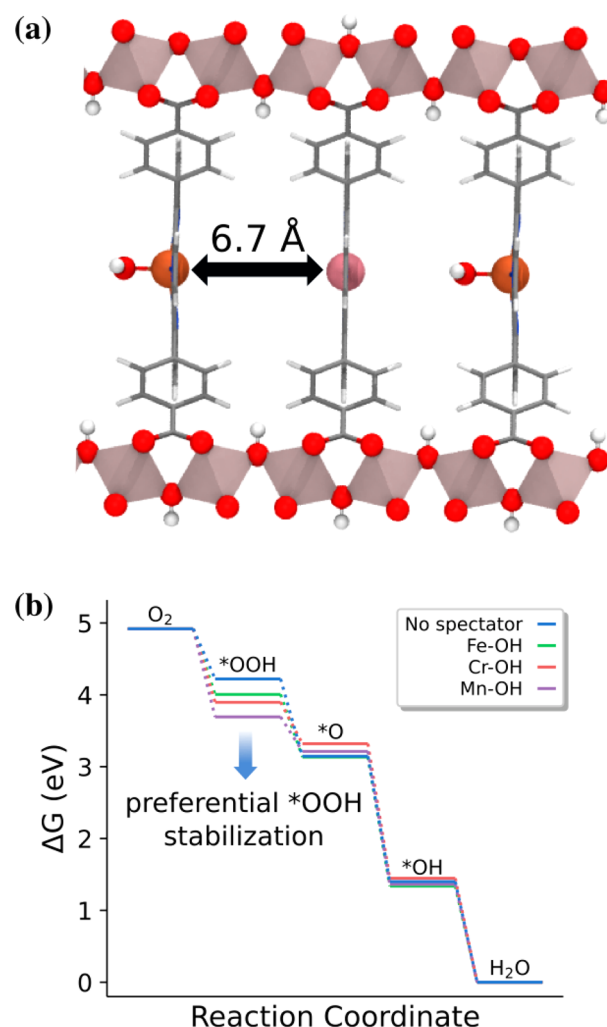

Figure 2. (a) Structure of bimetallic PMOF-Al with Co active site and Fe−OH spectator, (b) Free energy diagram (TPSSh-D3BJ) showing the preferential stabilization of *OOH. Color scheme: Co (pink), Fe (brown), C (gray), O (red), and H (white).
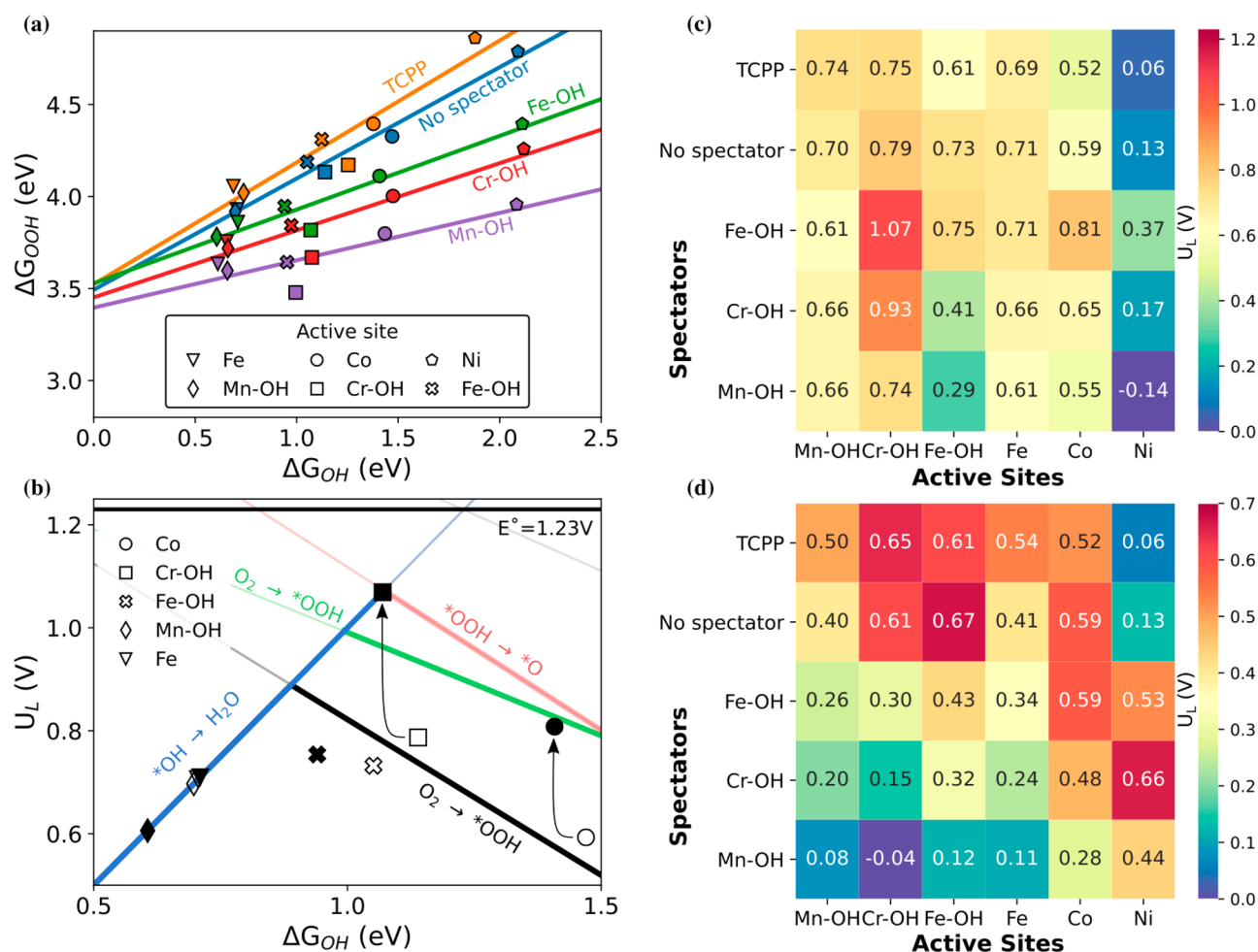
Figure 3. (a) Comparison of *OOH vs *OH scaling lines for TCPP, monometallic, and bimetallic PMOF-Al with different active sites and spectators, (b) 1-D volcano plot showing the improvement in activity (black arrows) due to the presence of Fe−OH spectator (filled symbols, red and green volcano legs) compared to the no spectator (empty symbols, black volcano leg) scenario. TPSSh-D3BJ calculated limiting potential for (c) 4e and (d) 2e ORR for various bimetallic MOFs.

porphyrin) stacked on top of each other to form a 3-D structure connected via a 1-D Al-oxide chain. PMOF-Al is water stable and has been shown to be experimentally active for ORR.[37] The spacing between the two linkers is ~6.7 Å, which compares well with the favorable region in Figure 1. As different linkers can be incorporated in MOFs during synthesis or using postsynthetic methods,[52−54] we used DFT calculations to explore mixed-linker PMOF-Al configurations consisting of alternating TM_1/TCPP and TM_2/TCPP linkers (TM_1 = Cr, Mn, Fe, Co, Ni; TM_2 = Cr, Mn, Fe). Pourbaix diagrams are used to determine the coverage and oxidation states of the TMs while allowing simultaneous binding on both sides of the linker (Figure S3). All possible spin combinations are explored to determine the lowest energy electronic structure for each TM (Table S1). Entropic corrections are calculated using the harmonic approximation (Table S2), and solvation contributions are estimated using VASPsol.[55] The solvent isosurface (Figure S4) confirms that the solvent penetrates the MOF cavity. Other solvation approaches are possible[56] but are beyond the scope of this work. The calculated absolute and relative solvation effects are summarized in Table S3.

Figure 2b shows the DFT-calculated free energy diagram for the Co active site in monometallic and bimetallic PMOF-Al

using the TPSSh-D3BJ[57] functional. The theoretical limiting potential for the molecular Co/TCPP analogue (U_L = 0.52 V) is consistent with the monometallic Co/PMOF system (U_L = 0.59 V, blue). Our calculated limiting potentials agree reasonably with the experimentally measured onset potentials (0.75 V),[37] further confirming the suitability of the computational protocol.

Similar calculations with RPBE-D3BJ predict incorrect spin states and TM geometry, while the HSE06-D3BJ functional underpredicts binding energies for Co/TCPP and Fe/TCPP. These findings are inconsistent with experimental results and are not discussed further (see the Supporting Information for details). Detailed benchmarking of different functionals (e.g., ωB97,[58] MN15,[59] and others[60]) with coupled cluster theory and/or multireference methods for various transition metals is beyond the scope of this work.[56,61−63]

Compared to Co-PMOF-Al with no spectator, Figure 2b shows that the presence of an oxophilic spectator (Fe−OH, green) improves the predicted activity. For instance, the theoretical limiting potential for the bimetallic Co/Fe−OH/ PMOF-Al catalyst (0.81 V) is comparable to the Pt/C benchmark (U_L = 0.8 V). The improved activity originates from the additional 0.22 eV stabilization of *OOH due to the presence of the Fe−OH spectator. Simulations of other

oxophilic TMs (see Mn−OH and Cr−OH in Figure 2b) confirm that the presence of the spectator ligand significantly affects *OOH binding; the other OXR adsorbates (i.e., *OH and *O) are largely unaffected.

While the above discussion is limited to the Co active site, we perform additional DFT calculations with Ni, Fe, Cr, and Mn active sites. For each TM, the most stable coverage predicted by the Pourbaix diagram is used (e.g., Cr−OH, Mn−OH). As shown in Figure 3a, we predict similar scaling slopes for TCPP (0.66, orange) and monometallic PMOF−Al (0.60, blue). The deviation from unity likely arises due to the changes in the spin states for *OOH and *OH intermediates and differences in the active site coordination geometry (e.g., square planar Co vs distorted square pyramidal Cr−OH). Previous work by Busch et al. has shown that the slope of the scaling line depends on the choice of the DFT functional.[60]

More interestingly, the presence of the Fe−OH spectator results in a favorable deviation from the above scaling behavior. Specifically, we observe a preferential *OOH stabilization of up to 0.4 eV for various TM active sites (Figure S5). A smaller deviation is observed for strongly binding TMs (e.g., Fe−*OOH, 0.07 eV). In contrast, weakly binding TMs (e.g., Ni−*OOH) are stabilized to a larger extent (0.39 eV). For a given TM active site, the extent of *OOH stabilization also depends on the identity of the spectator. For instance, Mn−OH spectator (purple, Figure 3a) results in systematically higher stabilization than Fe−OH spectator. In all cases, the *O and *OH binding energies do not change significantly (<0.15 eV).

The trends in *OOH stabilization can be explained by the increasing electronegativity of the spectating metal (Mn < Cr < Fe). Spectating metals with lower electronegativity allow for more charge to be localized on the spectator ligand (−OH), resulting in a stronger hydrogen bond and increased stability of the *OOH intermediate. Table S4 shows the differences in the calculated bond orders for Co active site with different spectators. In particular, the $H_{OOH}–O_{OH}$ bond order increases from 0.23 (Fe−OH spectator) to 0.33 (Mn−OH spectator), confirming a stronger hydrogen bond. Bond order analysis also reveals that the presence of the spectator localizes more charge on the *OOH adsorbate compared to the no spectator system. The $Co–O_{OOH}$ bond order decreases from 0.57 to 0.48 with the Mn−OH spectator. Although the weakened TM−oxygen bond may favor the 2e pathway, detailed investigation of kinetic effects and product selectivity (i.e., H_2O_2 vs H_2O) is beyond the scope of this work.

As the spectator stabilizes *OOH, the improvement in the ORR limiting potential is well-explained by the 1-D volcano plot in Figure 3b. Specifically, for TMs that lie on the right leg of the volcano (i.e., activity is limited by $O_2 →$ *OOH), the spectator stabilizes *OOH, improves the *OOH vs *OH scaling, and favorably shifts the right leg of the volcano. This is depicted by black arrows in Figure 3b corresponding to an improvement in the activity of Co and Cr−OH active sites due to the Fe−OH spectator (green line, filled symbols) compared to the no spectator case (black line, empty symbols). The predicted limiting potential for the bimetallic Cr/Fe−PMOF−Al catalyst is 1.07 V, which exceeds the performance of the benchmark Pt/C catalyst (U_L = 0.8 eV). Our calculations with TPSSh-D3BJ suggest that the Cr−OH active site possesses high activity for all spectator combinations; the limiting potentials for Cr−OH TCPP (0.75 V) and no spectator (0.79 V) agree very well with the experimental half-wave potential

(0.77 V) of a recently reported Cr−N$_4$ catalyst.[64] The strongly binding metals on the left leg of the volcano (e.g., Mn−OH) do not benefit from the addition of the spectator, as *OOH formation is not limiting for these catalysts.

We emphasize that circumventing scaling relations via *OOH stabilization does not guarantee enhanced activity, and only catalysts in which the potential-determining step (i.e., the least thermodynamically favorable reaction step) involves *OOH are influenced by this approach.[65,66] Moreover, although the potential-dependent step has been shown to correlate with kinetics,[6,67,68] it may not provide a quantitative description of the reaction rates.[69−72]

These results are further summarized in the heat-map in Figure 3c, which includes Mn−OH and Cr−OH spectators. While the Fe−OH spectator tends to improve the 4e limiting potentials, Mn−OH and Cr−OH do not have the same effect. Specifically, Mn−OH and Cr−OH overstabilize *OOH, and the activity becomes limited by the *OOH → *O step (see 1-D volcanoes in Figure S7).

As the *OOH → *O step is often not limiting for metals and alloys, we emphasize that molecular and MOF-based ORR catalysts require a more careful analysis beyond the traditional *OOH vs *OH scaling for metals and alloys. Single atom M−N$_4$ catalysts only allow binding of the *O intermediate at the on-top site (as opposed to the more favorable hollow sites for metallic surfaces), which has already been shown to destabilize binding of *O.[73] This destabilization of *O combined with overstabilization of *OOH presents a new bottleneck for 4e ORR, where formation of *O from *OOH limits the achievable potential. While these effects are observed in all bimetallic combinations, the moderate stabilization of *OOH due to the Fe−OH spectator allows for an improvement in theoretical overpotential, notably for the Co and Cr−OH active center. However, stronger stabilization seen with Mn−OH and Cr−OH spectators yields a reduction in catalytic performance as *OOH is stabilized to the point where *O formation is unfavorable.

Recognizing that this *O destabilization relative to metal surfaces may compromise the selectivity of these systems toward the 4e reduction to water, we extend our analysis to the 2e oxygen reduction reaction to form hydrogen peroxide. Figure 3d summarizes the calculated 2e limiting potentials for all active site and spectator combinations. As expected, for stronger binding active sites that lie on the left leg of the volcano, incorporation of an oxophilic spectator overstabilizes *OOH and reduces the 2e ORR activity. However, for weakly binding metals on the far right of the volcano, a noticeable improvement in theoretical limiting potential is obtained. For the Ni active site, TPSSh-D3BJ predicts highly active limiting potentials of 0.53 (0.66) V when combined with Fe−OH (Cr−OH) spectators, which represents a 0.4 eV improvement over the no spectator scenario.

The above results indicate that porphyrin-based MOFs are a promising platform for tuning the binding energies of OXR adsorbates. Unlike metals and alloys where only the composition[74] or strain[75] can be varied, the 3-D active sites in MOFs offer a unique degree of control that is unavailable in other materials. Specifically, in addition to appropriately choosing the bimetallic system (i.e., TM$_1$ and TM$_2$), we can now potentially design MOF topologies to further tune the adsorbate binding energies for OXR.

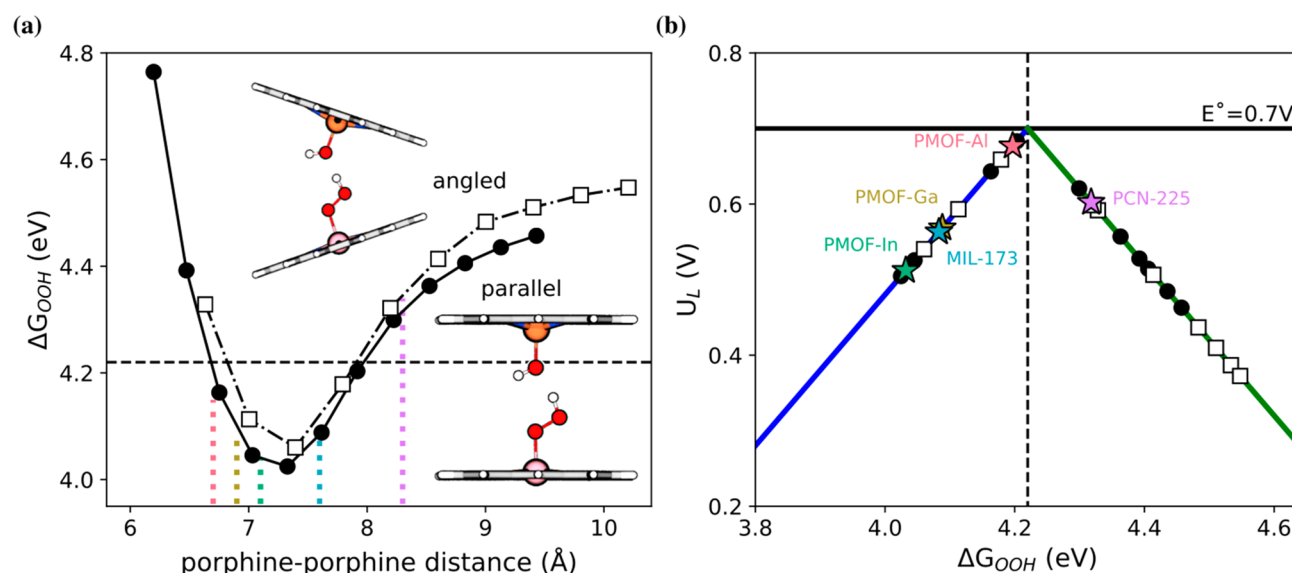As an illustrative example, we consider a model system consisting of two interacting porphine molecules (Co active

Figure 4. (a) *OOH binding energy for the two parallel (filled circles) and angled (empty squares) interacting porphine molecules at various distances. (b) TPSSh-D3BJ calculated 2e limiting potentials for the model systems. Limiting potentials for PMOF-Al (red), PMOF-Ga (yellow), PMOF-In (green), MIL-173 (blue), and PCN-225 (purple) are predicted from their measured porphyrin separation distance.

site, Fe−OH spectator) at varying distances. As shown in Figure 4a, parallel configurations can be considered as analogues of PMOF-Al with different 1-D metal oxide chains (e.g., substituting Al with Ga or In[76]), or other similar rod-based MOFs, such as MIL-173.[77] Additionally, a pair of angled (37°) porphines is chosen to mimic the topology of the porphyrinic Zr$_6$-oxo cluster MOF, PCN-225.[78] The distance between the TMs is varied to illustrate the reticular approach in MOF synthesis;[79] we demonstrate the effects of varying the linker size while retaining the same topology. Figure 4a shows a high degree of control on reaction thermodynamics can be achieved by tuning the separation distance between adjacent porphyrin motifs, and the distances of several known MOFs are highlighted with vertical dotted lines. For both the parallel and angled configurations, shorter distances (∼7 Å) enable stronger *OOH stabilization, which suggests a preference toward 4e ORR. Interestingly, TPSSh-D3BJ predicts a range of *OOH binding energies that encompass the 2e ORR optimum (4.2 eV, dashed black line in Figure 4). For the model systems considered here, we find that intrinsic catalytic activity is insensitive to small topological changes in porphyrin orientation (i.e., parallel versus angled). These results show that weakly *OOH binding active sites can be optimized for 2e peroxide synthesis by appropriately choosing the spectator transition metal, optimizing the TM$_1$−TM$_2$ separation, and changing the MOF topology. We acknowledge that these results alone are not conclusive of reaction selectivity; detailed kinetic studies and experimental measurements are necessary to validate our predictions.

By using state-of-the-art DFT calculations, we have demonstrated that porphyrin-based MOFs are an ideal materials platform for rationally designing 3-D active site environments for ORR. To the best of our knowledge, these computational predictions represent the first experimentally synthesizable heterogeneous catalysts (i.e., MOFs) where the 3-D structure of the active site can be intentionally designed to circumvent the *OOH vs *OH scaling relations. In addition to possible electrochemical stability concerns, other factors that impact the efficacy of MOF electrocatalysts, such as charge

transport,[80−83] counterion and substrate diffusion,[82,83] explicit solvation,[56] etc. represent ongoing research directions in the group. We anticipate that this work will motivate further computational studies and experimental validation of MOF-based electrocatalysts for ORR.

■ COMPUTATIONAL METHODS

Periodic density functional theory (DFT) calculations are performed using the projector augmented wave method as implemented in the Vienna ab initio simulation package (VASP). All energies are calculated using a 400 eV plane-wave cutoff. Only the Γ-point is sampled owing to the large MOF unit cells. A range of generalized gradient approximation (BEEF-vdW,[22] BLYP,[24,25] RPBE[23]) and hybrid (B3LYP,[26] HSE06,[27,28] and TPSSh[57]) functionals are used to examine the sensitivity of our results. Dispersion corrections are considered using the DFT-D3 method with Becke−Johnson damping.[29−31] Electronic energies are converged to 10^{-6} eV. All structures are relaxed until the forces are less than 0.03 eV/Å for RPBE and 0.1 eV/Å for HSE06 and TPSSh. A lower convergence threshold is used for the hybrid functionals owing to the high computational costs; differences in binding energies are less than 0.01 eV. Full relaxations are performed for RPBE and HSE06. TPSSh relaxations are performed with HSE06 geometry, only the M−N$_4$ atoms and the adsorbates are allowed to relax. All possible spin states are considered. Implicit solvation corrections are implemented using VAS-PSol.[55] The finite displacement method (0.015 Å) is used to calculate the entropic corrections and zero-point energies. Bond orders are calculated using the density derived electrostatic and chemical (DDEC) charge method.[84,85]

■ ASSOCIATED CONTENT

ⓢ Supporting Information

The Supporting Information is available free of charge at https://pubs.acs.org/doi/10.1021/acs.jpclett.0c02889.

    Computational details, functional dependency and Van der Waals contributions, binding energy differences, Pourbaix diagrams, spin-state energies, free energy

corrections, solvent isosurface, implicit solvation effects, stabilization of *OOH, *O, and *OH, H-bond interactions and bond orders, volcano plots, justification of TPSSh-D3BJ, functional comparison for *OOH binding, theoretical limiting potentials, and *OOH vs *OH scaling (PDF)

Atomic Simulation Environment database of DFT-optimized structures calculated using the TPSSh-D3BJ functional (DB)

Details on accessing the data (ZIP)

■ AUTHOR INFORMATION

Corresponding Authors

Samira Siahrostami − *Department of Chemistry, University of Calgary, Calgary, Alberta T2N 1N4, Canada;* ⓘ orcid.org/0000-0002-1192-4634; Email: samira.siahrostami@ucalgary.ca

Ambarish Kulkarni − *Department of Chemical Engineering, University of California, Davis, Davis, California 95616, United States;* ⓘ orcid.org/0000-0001-9834-8264; Email: arkulkarni@ucdavis.edu

Authors

Tyler Sours − *Department of Chemical Engineering, University of California, Davis, Davis, California 95616, United States*

Anjli Patel − *SUNCAT Center for Interface Science and Catalysis, Department of Chemical Engineering, Stanford University, Stanford, California 94305, United States;* ⓘ orcid.org/0000-0002-0590-7619

Jens Nørskov − *Department of Physics, Technical University of Denmark, 2800 Kongens Lyngby, Denmark;* ⓘ orcid.org/0000-0002-4427-7728

Complete contact information is available at:
https://pubs.acs.org/10.1021/acs.jpclett.0c02889

Author Contributions

#T.S. and A.P. contributed equally to this work.

■ REFERENCES

(1) Debe, M. K. Electrocatalyst Approaches and Challenges for Automotive Fuel Cells. *Nature* **2012**, *486* (7401), 43−51.

(2) Seh, Z. W.; Kibsgaard, J.; Dickens, C. F.; Chorkendorff, I.; Nørskov, J. K.; Jaramillo, T. F. Combining Theory and Experiment in Electrocatalysis: Insights into Materials Design. *Science (Washington, DC, U. S.)* **2017**, *355* (6321), eaad4998.

(3) Lefèvre, M.; Proietti, E.; Jaouen, F.; Dodelet, J. P. Iron-Based Catalysts with Improved Oxygen Reduction Activity in Polymer Electrolyte Fuel Cells. *Science (Washington, DC, U. S.)* **2009**, *324* (5923), 71−74.

(4) Li, J.; Chen, M.; Cullen, D. A.; Hwang, S.; Wang, M.; Li, B.; Liu, K.; Karakalos, S.; Lucero, M.; Zhang, H.; Lei, C.; Xu, H.; Sterbinsky, G. E.; Feng, Z.; Su, D.; More, K. L.; Wang, G.; Wang, Z.; Wu, G. Atomically Dispersed Manganese Catalysts for Oxygen Reduction in Proton-Exchange Membrane Fuel Cells. *Nat. Catal.* **2018**, *1* (12), 935−945.

(5) Man, I. C.; Su, H. Y.; Calle-Vallejo, F.; Hansen, H. A.; Martínez, J. I.; Inoglu, N. G.; Kitchin, J.; Jaramillo, T. F.; Nørskov, J. K.; Rossmeisl, J. Universality in Oxygen Evolution Electrocatalysis on Oxide Surfaces. *ChemCatChem* **2011**, *3* (7), 1159−1165.

(6) Viswanathan, V.; Hansen, H. A.; Rossmeisl, J.; Nørskov, J. K. Universality in Oxygen Reduction Electrocatalysis on Metal Surfaces. *ACS Catal.* **2012**, *2* (8), 1654−1660.

(7) Chen, Y.; Ji, S.; Chen, C.; Peng, Q.; Wang, D.; Li, Y. Single-Atom Catalysts: Synthetic Strategies and Electrochemical Applications. *Joule* **2018**, *2* (7), 1242−1264.

(8) Wan, C.; Duan, X.; Huang, Y. Molecular Design of Single-Atom Catalysts for Oxygen Reduction Reaction. *Adv. Energy Mater.* **2020**, *10* (14), 1903815.

(9) Christensen, R.; Hansen, H. A.; Dickens, C. F.; Nørskov, J. K.; Vegge, T. Functional Independent Scaling Relation for ORR/OER Catalysts. *J. Phys. Chem. C* **2016**, *120* (43), 24910−24916.

(10) Song, F.; Bai, L.; Moysiadou, A.; Lee, S.; Hu, C.; Liardet, L.; Hu, X. Transition Metal Oxides as Electrocatalysts for the Oxygen Evolution Reaction in Alkaline Solutions: An Application-Inspired Renaissance. *J. Am. Chem. Soc.* **2018**, *140* (25), 7748−7759.

(11) Calle-Vallejo, F.; Martínez, J. I.; Rossmeisl, J. Density Functional Studies of Functionalized Graphitic Materials with Late Transition Metals for Oxygen Reduction Reactions. *Phys. Chem. Chem. Phys.* **2011**, *13* (34), 15639−15643.

(12) Kulkarni, A.; Siahrostami, S.; Patel, A.; Nørskov, J. K. Understanding Catalytic Activity Trends in the Oxygen Reduction Reaction. *Chem. Rev.* **2018**, *118* (5), 2302−2312.

(13) Tao, H. B.; Zhang, J.; Chen, J.; Zhang, L.; Xu, Y.; Chen, J. G.; Liu, B. Revealing Energetics of Surface Oxygen Redox from Kinetic Fingerprint in Oxygen Electrocatalysis. *J. Am. Chem. Soc.* **2019**, *141* (35), 13803−13811.

(14) Koper, M. T. M. Thermodynamic Theory of Multi-Electron Transfer Reactions: Implications for Electrocatalysis. *J. Electroanal. Chem.* **2011**, *660* (2), 254−260.

(15) Vojvodic, A.; Nørskov, J. K. New Design Paradigm for Heterogeneous Catalysts. *Natl. Sci. Rev.* **2015**, *2* (2), 140−143.

(16) Wan, H.; Østergaard, T. M.; Arnarson, L.; Rossmeisl, J. Climbing the 3D Volcano for the Oxygen Reduction Reaction Using Porphyrin Motifs. *ACS Sustainable Chem. Eng.* **2019**, *7* (1), 611−617.

(17) Wan, H.; Jensen, A. W.; Escudero-Escribano, M.; Rossmeisl, J. Insights in the Oxygen Reduction Reaction: From Metallic Electrocatalysts to Diporphyrins. *ACS Catal.* **2020**, *10* (11), 5979−5989.

(18) Govindarajan, N.; Koper, M. T. M.; Meijer, E. J.; Calle-Vallejo, F. Outlining the Scaling-Based and Scaling-Free Optimization of Electrocatalysts. *ACS Catal.* **2019**, *9* (5), 4218−4225.

(19) Chang, C. K.; Liu, H. Y.; Abdalmuhdi, I.; Liu, H. Y. Electroreduction of Oxygen by Pillared Cobalt Cofacial Diporphyrin Catalysts. *J. Am. Chem. Soc.* **1984**, *106* (9), 2725−2726.

(20) Collman, J. P.; Wagenknecht, P. S.; Hutchison, J. E. Molecular Catalysts for Multielectron Redox Reactions of Small Molecules: The "Cofacial Metallodiporphyrin" Approach. *Angew. Chem., Int. Ed. Engl.* **1994**, *33* (15−16), 1537−1554.

(21) Rosenthal, J.; Nocera, D. G. Role of Proton-Coupled Electron Transfer in O-O Bond Activation. *Acc. Chem. Res.* **2007**, *40* (7), 543−553.

(22) Wellendorff, J.; Silbaugh, T. L.; Garcia-Pintos, D.; Nørskov, J. K.; Bligaard, T.; Studt, F.; Campbell, C. T. A Benchmark Database for Adsorption Bond Energies to Transition Metal Surfaces and Comparison to Selected {DFT} Functionals. *Surf. Sci.* **2015**, *640*, 36−44.

(23) Hammer, B.; Hansen, L. B.; Nørskov, J. K. Improved Adsorption Energetics within Density-Functional Theory Using Revised Perdew-Burke-Ernzerhof Functionals. *Phys. Rev. B: Condens. Matter Mater. Phys.* **1999**, *59* (11), 7413−7421.

(24) Becke, A. D. Density-Functional Exchange-Energy Approximation with Correct Asymptotic Behavior. *Phys. Rev. A: At., Mol., Opt. Phys.* **1988**, *38* (6), 3098−3100.

(25) Lee, C.; Yang, W.; Parr, R. G. Development of the Colle-Salvetti Correlation-Energy Formula into a Functional of the Electron Density. *Phys. Rev. B: Condens. Matter Mater. Phys.* **1988**, *37* (2), 785−789.

(26) Stephens, P. J.; Devlin, F. J.; Chabalowski, C. F.; Frisch, M. J. Ab Initio Calculation of Vibrational Absorption and Circular Dichroism Spectra Using Density Functional Force Fields. *J. Phys. Chem.* **1994**, *98* (45), 11623−11627.

(27) Heyd, J.; Scuseria, G. E.; Ernzerhof, M. Hybrid Functionals Based on a Screened Coulomb Potential. *J. Chem. Phys.* **2003**, *118* (18), 8207−8215.

(28) Krukau, A. V.; Vydrov, O. A.; Izmaylov, A. F.; Scuseria, G. E. Influence of the Exchange Screening Parameter on the Performance of Screened Hybrid Functionals. *J. Chem. Phys.* **2006**, *125* (22), 224106.

(29) Grimme, S.; Antony, J.; Ehrlich, S.; Krieg, H. A Consistent and Accurate Ab Initio Parametrization of Density Functional Dispersion Correction (DFT-D) for the 94 Elements H-Pu. *J. Chem. Phys.* **2010**, *132* (15), 154104.

(30) Grimme, S.; Ehrlich, S.; Goerigk, L. Effect of the Damping Function in Dispersion Corrected Density Functional Theory. *J. Comput. Chem.* **2011**, *32* (7), 1456−1465.

(31) Smith, D. G. A.; Burns, L. A.; Patkowski, K.; Sherrill, C. D. Revised Damping Parameters for the D3 Dispersion Correction to Density Functional Theory. *J. Phys. Chem. Lett.* **2016**, *7* (12), 2197−2203.

(32) Rosen, A. S.; Notestein, J. M.; Snurr, R. Q. Structure-Activity Relationships That Identify Metal-Organic Framework Catalysts for Methane Activation. *ACS Catal.* **2019**, *9* (4), 3576−3587.

(33) Szécsényi, Á.; Khramenkova, E.; Chernyshov, I. Y.; Li, G.; Gascon, J.; Pidko, E. A. Breaking Linear Scaling Relationships with Secondary Interactions in Confined Space: A Case Study of Methane Oxidation by Fe/ZSM-5 Zeolite. *ACS Catal.* **2019**, *9* (10), 9276−9284.

(34) Tranchemontagne, D. J.; Tranchemontagne, J. L.; O'keeffe, M.; Yaghi, O. M. Secondary Building Units, Nets and Bonding in the Chemistry of Metal-Organic Frameworks. *Chem. Soc. Rev.* **2009**, *38* (5), 1257−1283.

(35) Schoedel, A.; Li, M.; Li, D.; O'Keeffe, M.; Yaghi, O. M. Structures of Metal-Organic Frameworks with Rod Secondary Building Units. *Chem. Rev.* **2016**, *116* (19), 12466−12535.

(36) Lu, W.; Wei, Z.; Gu, Z. Y.; Liu, T. F.; Park, J.; Park, J.; Tian, J.; Zhang, M.; Zhang, Q.; Gentle, T.; Bosch, M.; Zhou, H. C. Tuning the Structure and Function of Metal-Organic Frameworks via Linker Design. *Chem. Soc. Rev.* **2014**, *43* (16), 5561−5593.

(37) Lions, M.; Tomasino, J.-B.; Chattot, R.; Abeykoon, B.; Guillou, N.; Devic, T.; Demessence, A.; Cardenas, L.; Maillard, F.; Fateeva, A.; Tommasino, J.-B.; Chattot, R.; Abeykoon, B.; Guillou, N.; Devic, T.; Demessence, A.; Cardenas, L.; Maillard, F.; Fateeva, A. Insights into the Mechanism of Electrocatalysis of Oxygen Reduction Reaction by a Porphyrinic Metal Organic Framework. *Chem. Commun.* **2017**, *53* (48), 6496−6499.

(38) Usov, P. M.; Huffman, B.; Epley, C. C.; Kessinger, M. C.; Zhu, J.; Maza, W. A.; Morris, A. J. Study of Electrocatalytic Properties of Metal-Organic Framework PCN-223 for the Oxygen Reduction Reaction. *ACS Appl. Mater. Interfaces* **2017**, *9* (39), 33539−33543.

(39) Cichocka, M. O.; Liang, Z.; Feng, D.; Back, S.; Siahrostami, S.; Wang, X.; Samperisi, L.; Sun, Y.; Xu, H.; Hedin, N.; Zheng, H.; Zou, X.; Zhou, H.-C.; Huang, Z. A Porphyrinic Zirconium Metal-Organic Framework for Oxygen Reduction Reaction: Tailoring the Spacing between Active-Sites through Chain-Based Inorganic Building Units. *J. Am. Chem. Soc.* **2020**, *142* (36), 15386−15395.

(40) Miner, E. M.; Fukushima, T.; Sheberla, D.; Sun, L.; Surendranath, Y.; Dinca, M. Electrochemical Oxygen Reduction Catalysed by Ni3(Hexaiminotriphenylene)2. *Nat. Commun.* **2016**, *7*, 1−7.

(41) Xu, Y.; Li, Q.; Xue, H.; Pang, H. Metal-Organic Frameworks for Direct Electrochemical Applications. *Coord. Chem. Rev.* **2018**, *376*, 292−318.

(42) D'Alessandro, D. M. Exploiting Redox Activity in Metal-Organic Frameworks: Concepts, Trends and Perspectives. *Chem. Commun.* **2016**, *52* (58), 8957−8971.

(43) Solomon, M. B.; Church, T. L.; D'Alessandro, D. M. Perspectives on Metal-Organic Frameworks with Intrinsic Electrocatalytic Activity. *CrystEngComm* **2017**, *19* (29), 4049−4065.

(44) Downes, C. A.; Marinescu, S. C. Electrocatalytic Metal-Organic Frameworks for Energy Applications. *ChemSusChem* **2017**, *10* (22), 4374−4392.

(45) Wang, W.; Xu, X.; Zhou, W.; Shao, Z. Recent Progress in Metal-Organic Frameworks for Applications in Electrocatalytic and Photocatalytic Water Splitting. *Adv. Sci.* **2017**, *4* (4), 1600371.

(46) Chen, R.; Li, H.; Chu, D.; Wang, G. Unraveling Oxygen Reduction Reaction Mechanisms on Carbon-Supported Fe-Phthalocyanine and Co-Phthalocyanine Catalysts in Alkaline Solutions. *J. Phys. Chem. C* **2009**, *113* (48), 20689−20697.

(47) Busch, M. Water Oxidation: From Mechanisms to Limitations. *Curr. Opin. Electrochem.* **2018**, *9*, 278−284.

(48) Kattel, S.; Atanassov, P.; Kiefer, B. A Density Functional Theory Study of Oxygen Reduction Reaction on Non-PGM Fe-Nx-C Electrocatalysts. *Phys. Chem. Chem. Phys.* **2014**, *16* (27), 13800−13806.

(49) Cao, H.; Xia, G. J.; Chen, J. W.; Yan, H. M.; Huang, Z.; Wang, Y. G. Mechanistic Insight into the Oxygen Reduction Reaction on the Mn-N4/C Single-Atom Catalyst: The Role of the Solvent Environment. *J. Phys. Chem. C* **2020**, *124* (13), 7287−7294.

(50) Zhong, L.; Li, S. Unconventional Oxygen Reduction Reaction Mechanism and Scaling Relation on Single-Atom Catalysts. *ACS Catal.* **2020**, *10* (7), 4313−4318.

(51) Fateeva, A.; Chater, P. A.; Ireland, C. P.; Tahir, A. A.; Khimyak, Y. Z.; Wiper, P. V.; Darwent, J. R.; Rosseinsky, M. J. A Water-Stable Porphyrin-Based Metal-Organic Framework Active for Visible-Light Photocatalysis. *Angew. Chem., Int. Ed.* **2012**, *51* (30), 7440−7444.

(52) Wang, Z.; Cohen, S. M. Postsynthetic Modification of Metal-Organic Frameworks. *Chem. Soc. Rev.* **2009**, *38* (5), 1315−1329.

(53) Tanabe, K. K.; Cohen, S. M. Postsynthetic Modification of Metal-Organic Frameworks—a Progress Report. *Chem. Soc. Rev.* **2011**, *40* (2), 498−519.

(54) Kim, M.; Cahill, J. F.; Su, Y.; Prather, K. A.; Cohen, S. M. Postsynthetic Ligand Exchange as a Route to Functionalization of "inert" Metal-Organic Frameworks. *Chem. Sci.* **2012**, *3* (1), 126−130.

(55) Mathew, K.; Hennig, R. G. Implicit Self-Consistent Description of Electrolyte in Plane-Wave Density-Functional Theory. *arXiv.org:1601.03346*, **2016**.

(56) Patel, A. M.; Ringe, S.; Siahrostami, S.; Bajdich, M.; Nørskov, J. K.; Kulkarni, A. R. Theoretical Approaches to Describing the Oxygen Reduction Reaction Activity of Single-Atom Catalysts. *J. Phys. Chem. C* **2018**, *122* (51), 29307−29318.

(57) Staroverov, V. N.; Scuseria, G. E.; Tao, J.; Perdew, J. P. Comparative Assessment of a New Nonempirical Density Functional: Molecules and Hydrogen-Bonded Complexes. *J. Chem. Phys.* **2003**, *119* (23), 12129−12137.

(58) Chai Da, J.; Head-Gordon, M. Systematic Optimization of Long-Range Corrected Hybrid Density Functionals. *J. Chem. Phys.* **2008**, *128* (8), 084106.

(59) Yu, H. S.; He, X.; Li, S. L.; Truhlar, D. G. MN15: A Kohn-Sham Global-Hybrid Exchange-Correlation Density Functional with

Broad Accuracy for Multi-Reference and Single-Reference Systems and Noncovalent Interactions. *Chem. Sci.* **2016**, 7 (8), 5032−5051.

(60) Busch, M.; Fabrizio, A.; Luber, S.; Hutter, J.; Corminboeuf, C. Exploring the Limitation of Molecular Water Oxidation Catalysts. *J. Phys. Chem. C* **2018**, 122 (23), 12404−12412.

(61) Gaggioli, C. A.; Stoneburner, S. J.; Cramer, C. J.; Gagliardi, L. Beyond Density Functional Theory: The Multiconfigurational Approach to Model Heterogeneous Catalysis. *ACS Catal.* **2019**, 9 (9), 8481−8502.

(62) Radoń, M.; Pierloot, K. Binding of CO, NO, and O2 to Heme by Density Functional and Multireference Ab Initio Calculations. *J. Phys. Chem. A* **2008**, 112 (46), 11824−11832.

(63) Radoń, M. Spin-State Energetics of Heme-Related Models from DFT and Coupled Cluster Calculations. *J. Chem. Theory Comput.* **2014**, 10 (6), 2306−2321.

(64) Luo, E.; Zhang, H.; Wang, X.; Gao, L.; Gong, L.; Zhao, T.; Jin, Z.; Ge, J.; Jiang, Z.; Liu, C.; Xing, W. Single-Atom Cr-N4 Sites Designed for Durable Oxygen Reduction Catalysis in Acid Media. *Angew. Chem., Int. Ed.* **2019**, 58 (36), 12469−12475.

(65) Govindarajan, N.; García-Lastra, J. M.; Meijer, E. J.; Calle-Vallejo, F. Does the Breaking of Adsorption-Energy Scaling Relations Guarantee Enhanced Electrocatalysis? *Curr. Opin. Electrochem.* **2018**, 8, 110−117.

(66) Piqué, O.; Illas, F.; Calle-Vallejo, F. Designing Water Splitting Catalysts Using Rules of Thumb: Advantages, Dangers and Alternatives. *Phys. Chem. Chem. Phys.* **2020**, 22 (13), 6797−6803.

(67) Hansen, H. A.; Viswanathan, V.; NØrskov, J. K. Unifying Kinetic and Thermodynamic Analysis of 2 E- and 4 e - Reduction of Oxygen on Metal Surfaces. *J. Phys. Chem. C* **2014**, 118 (13), 6706−6718.

(68) Koper, M. T. M. Analysis of Electrocatalytic Reaction Schemes: Distinction between Rate-Determining and Potential-Determining Steps. *J. Solid State Electrochem.* **2013**, 17 (2), 339−344.

(69) Exner, K. S.; Over, H. Kinetics of Electrocatalytic Reactions from First-Principles: A Critical Comparison with the Ab Initio Thermodynamics Approach. *Acc. Chem. Res.* **2017**, 50 (5), 1240−1247.

(70) Exner, K. S. Beyond the Traditional Volcano Concept: Overpotential-Dependent Volcano Plots Exemplified by the Chlorine Evolution Reaction over Transition-Metal Oxides. *J. Phys. Chem. C* **2019**, 123 (27), 16921−16928.

(71) Exner, K. S. A Universal Descriptor for the Screening of Electrode Materials for Multiple-Electron Processes: Beyond the Thermodynamic Overpotential. *ACS Catal.* **2020**, 12607−12617.

(72) Exner, K. S.; Sohrabnejad-Eskan, I.; Over, H. A Universal Approach to Determine the Free Energy Diagram of an Electrocatalytic Reaction. *ACS Catal.* **2018**, 8 (3), 1864−1879.

(73) Yang, S.; Verdaguer-Casadevall, A.; Arnarson, L.; Silvioli, L.; Colić, V.; Frydendal, R.; Rossmeisl, J.; Chorkendorff, I.; Stephens, I. E. L. Toward the Decentralized Electrochemical Production of H2O2: A Focus on the Catalysis. *ACS Catal.* **2018**, 8 (5), 4064−4081.

(74) Mukerjee, S.; Srinivasan, S.; Soriaga, M. P.; McBreen, J. Role of Structural and Electronic Properties of Pt and Pt Alloys on Electrocatalysis of Oxygen Reduction: An In Situ XANES and EXAFS Investigation. *J. Electrochem. Soc.* **1995**, 142 (5), 1409−1422.

(75) Escudero-Escribano, M.; Malacrida, P.; Hansen, M. H.; Vej-Hansen, U. G.; Velazquez-Palenzuela, A.; Tripkovic, V.; Schiotz, J.; Rossmeisl, J.; Stephens, I. E. L.; Chorkendorff, I. Tuning the Activity of Pt Alloy Electrocatalysts by Means of the Lanthanide Contraction. *Science (Washington, DC, U. S.)* **2016**, 352 (6281), 73−76.

(76) Rhauderwiek, T.; Waitschat, S.; Wuttke, S.; Reinsch, H.; Bein, T.; Stock, N. Nanoscale Synthesis of Two Porphyrin-Based MOFs with Gallium and Indium. *Inorg. Chem.* **2016**, 55 (11), 5312−5319.

(77) Mouchaham, G.; Abeykoon, B.; Giménez-Marqués, M.; Navalon, S.; Santiago-Portillo, A.; Affram, M.; Guillou, N.; Martineau, C.; Garcia, H.; Fateeva, A.; Devic, T. Adaptability of the Metal(III,IV) 1,2,3-Trioxobenzene Rod Secondary Building Unit for the Production of Chemically Stable and Catalytically ActIVe MOFs. *Chem. Commun.* **2017**, 53 (54), 7661−7664.

(78) Jiang, H. L.; Feng, D.; Wang, K.; Gu, Z. Y.; Wei, Z.; Chen, Y. P.; Zhou, H. C. An Exceptionally Stable, Porphyrinic Zr Metal-Organic Framework Exhibiting PH-Dependent Fluorescence. *J. Am. Chem. Soc.* **2013**, 135 (37), 13934−13938.

(79) Yaghi, O. M.; O'Keeffe, M.; Ockwig, N. W.; Chae, H. K.; Eddaoudi, M.; Kim, J. Reticular Synthesis and the Design of New Materials. *Nature* **2003**, 423, 705−714.

(80) Pratik, S. M.; Gagliardi, L.; Cramer, C. J. Engineering Electrical Conductivity in Stable Zirconium-Based PCN-222 MOFs with Permanent Mesoporosity. *Chem. Mater.* **2020**, 32 (14), 6137−6149.

(81) Patwardhan, S.; Schatz, G. C. Theoretical Investigation of Charge Transfer in Metal Organic Frameworks for Electrochemical Device Applications. *J. Phys. Chem. C* **2015**, 119 (43), 24238−24247.

(82) Cai, M.; Loague, Q.; Morris, A. J. Design Rules for Efficient Charge Transfer in Metal-Organic Framework Films: The Pore Size Effect. *J. Phys. Chem. Lett.* **2020**, 11 (3), 702−709.

(83) Liberman, I.; Shimoni, R.; Ifraemov, R.; Rozenberg, I.; Singh, C.; Hod, I. Active-Site Modulation in an Fe-Porphyrin-Based Metal-Organic Framework through Ligand Axial Coordination: Accelerating Electrocatalysis and Charge-Transport Kinetics. *J. Am. Chem. Soc.* **2020**, 142 (4), 1933−1940.

(84) Manz, T. A.; Sholl, D. S. Chemically Meaningful Atomic Charges That Reproduce the Electrostatic Potential in Periodic and Nonperiodic Materials. *J. Chem. Theory Comput.* **2010**, 6 (8), 2455−2468.

(85) Manz, T. A. Introducing DDEC6 Atomic Population Analysis: Part 3. Comprehensive Method to Compute Bond Orders. *RSC Adv.* **2017**, 7 (72), 45552−45581.